SAND2011-9473 C
SAND2011-9473C

Code verification for the extended finite element method: the compound cohesionless impact problem

John H. J. Niederhaus*, Marlin E. Kipp, S. J. Mosso, Thomas E. Voth

Computational Shock and Multiphysics Department, Sandia National Laboratories, Albuquerque, NM, USA 87185

Abstract

Wave propagation during impact of three solid bodies is modeled numerically for verification purposes. Difficulties arising in Eulerian simulations for this problem are outlined. Analytic solutions are reviewed for impact in copper at 10 and 1000 m/s in a contrived scenario where dissipation is absent. For impact between copper and aluminum at 100 m/s, with dissipative effects included, reference solutions are obtained using a method-of-characteristics-based technique. With the shock hydrodynamics code ALEGRA, solutions are computed using Lagrangian and Eulerian methods, and using an alternative extended finite element method (XFEM) formulation. Code verification using spatial refinement shows that acceptable convergence behavior in Eulerian simulations is obtained only with XFEM.

Keywords: impact, XFEM, verification
2000 MSC: 46.15.-x

1. Compound cohesionless impact: dissipationless

We consider here in one spatial dimension the impact of a solid projectile on a compound, cohesionless solid target. The target is composed of two pieces joined at a cohesionless interface. A projectile incident from the left

*Corresponding author.
Email address: jhniede@sandia.gov (John H. J. Niederhaus)

[1]Sandia National Laboratories is a multi-program laboratory managed and operated by Sandia Corporation, a wholly owned subsidiary of Lockheed Martin Corporation, for the U.S. Department of Energy's National Nuclear Security Administration under contract DE-AC04-94AL85000.

strikes the left surface of the initially stationary target, as shown in Figure 1, generating forward and backward waves in the projectile and target. These waves undergo a series of interface interactions with free surfaces or material interfaces on the projectile or target, each giving rise to reflected and transmitted waves of compression or release. These waves mediate the transfer of momentum from the projectile to the target.

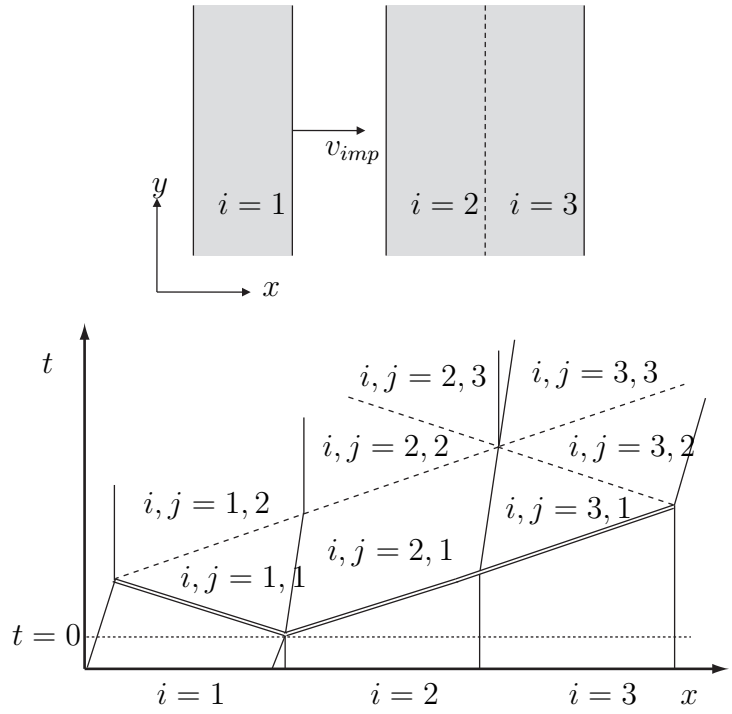

Figure 1: One-dimensional impact on a compound cohesionless target: schematic x-t diagram showing wave propagation pattern for 1D symmetric, cohesionless impact for three bodies of the same composition.

The evolution of the system can be visualized easily by considering the succession of compression and release waves that arise in the three bodies or plates, as shown in Figure 1. The plates are indexed by $i = 1, 2, 3$, and the successive states by $j = 1, 2, 3, \ldots$. Thus, the pair (i, j) indicates a unique region in the x-t plane bounded by compression or rarefaction waves and material interfaces. Compression waves are indicated by double lines, release waves by dashed lines, and material surfaces by solid lines.

For simplicity and clarity, we ignore wave splitting effects associated with plasticity, phase changes, and tensile failure, and we ignore the spreading over time of the release wave fronts. Further, we assume that all three plates have equal thickness and identical composition, and therefore refer to the impact event as "symmetric" in this sense.

The initial impact event at velocity v_{imp} generates a forward compression wave in plate 2 and a backward compression wave in plate 1. Both waves reflect at free surfaces: the forward wave at the rear of plate 3 after passing unchanged across the cohesionless interface, and the backward wave at the front of plate 1. Release waves then propagate inward.

As indicated in the diagram in Figure 1, the arrival of these release waves at the cohesionless interface between plates 2 and 3 results in separation of the plates, since the interface cannot sustain tension. The recoil velocity of the rear plate is therefore encoded in the particle velocity of the shock state $i, j = 3, 3$. This implies that the rear-plate recoil velocity can be obtained simply by tracing shock and release states from initial impact through the various transmissions and reflections, up to the $i, j = 3, 3$ region of the x-t plot. Exact or highly accurate solutions can therefore be obtained, and the problem can be used for verification of numerical methods for multimaterial shock hydrodynamics. This is the work undertaken in the present study.

A particularly simple outcome emerges in the special case where not only wave-splitting effects, but all dissipative effects are neglected. To make the problem dissipationless, we apply several assumptions regarding the response of the material. We assume that the thermal contribution to the pressure is negligible, and the pressure is determined solely by the volumetric contribution – that is, by the Hugoniot. We also assume that the material response is purely elastic and free from tensile failure throughout the event, so that neither plasticity nor damage play a role. In this case, conservation of momentum and energy dictate that the rear plate must recoil with exactly the initial impact velocity: $v_{rec} = u_{3,3} = v_{imp}$. This problem is a one-dimensional analog of the demonstration often referred to "Newton's cradle."

For the present study, we use the ambient density and sound speed of copper to characterize the medium: $\rho_0 = 8930$ kg/m^3, $c_0 = 3940$ m/s, with other properties represented using a Mie-Grüneisen equation of state (EOS) model. In order to eliminate thermal contributions to the pressure, we zero the Grüneisen coefficient for our modified copper: $\Gamma_0 = 0$. In order to eliminate the dissipation introduced by shock waves themselves, we must ensure that shocks and release waves follow the same path in pressure-volume

space. One means of ensuring this is to impose the restriction that the shock wave speed is fixed with respect to the particle speed. Thus, we modify the linear u_s-u_p relationship between the shock wave speed u_s and the particle speed u_p, setting the linear coefficient $s = 0$ such that the shock wave speed is fixed: $u_s = c_0 + su_p = c_0$. In this case, the Hugoniot is linear in pressure-volume space: $\partial p/\partial V = c_0^2 = \text{const}$. This implies $\partial^2 p/\partial V^2 = 0$, so that entropy is constant on the Hugoniot.

With this set of approximations, we may regard the system as dissipationless. To further clarify the consequences of these assumptions, we sketch the evolution of the state of the three plates in pressure-velocity (p-u) space in Figure 2. Here the three points A, B, and C indicate the initial undisturbed, stationary state; the shock state; and the initial projectile state, respectively. The points are connected by lines which indicate passage from one state to another. Though these lines do not necessarily trace the actual path followed during loading and unloading, they are representative of loading (compression) and unloading (release) transitions for each plate. Under the assumptions just listed, the material must follow a path of identical slope in both compression and release. Otherwise, when plotted in pressure-volume space, the area between the two paths would be nonzero and the load-unload process would be dissipative. Therefore the loading/unloading path slopes in Figure 2 are shown as identical in compression and release. Plate 1 follows the path CBA, plate 2 follows ABA, and plate 3 follows ABC. In particular, under these assumptions, the path of plate 3 must terminate at point C. The symmetry of the loading/unloading processes thus requires that the rear-plate recoil velocity be equal to the impact velocity, and that plates 1 and 2 relax to zero velocity and zero pressure after unloading.

In practice, at the impact speeds considered here, plasticity, fracture, and nonlinear wave propagation clearly cannot be neglected. Therefore, it is important to recognize that the assumptions applied here, while convenient for mathematical purposes, are not physically realistic. Nevertheless, numerical methods used to solve the problem should reproduce the exact solution for these conditions.

2. Verification analysis: dissipationless

The compound cohesionless impact problem with these "dissipationless" restrictions is simulated here using the arbitrary Lagrangian-Eulerian (ALE) shock hydrodynamics code ALEGRA [1]. ALEGRA uses the finite element

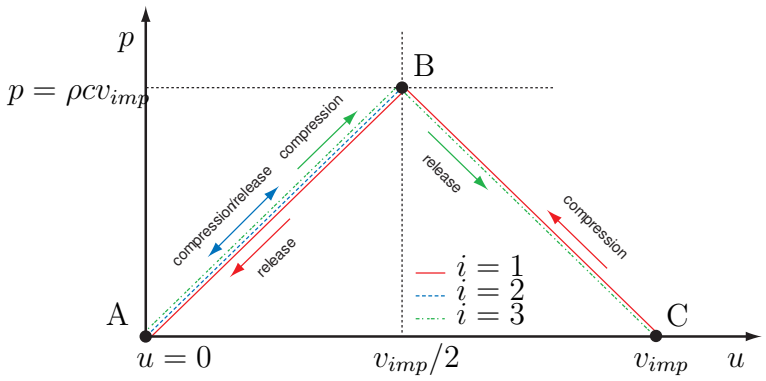

Figure 2: Representative loading and unloading transitions in pressure-velocity (p-u) space for the three plates included in the cohesionless impact problem. Point A: initial stationary state; point B: shock state; point C: initial projectile state.

method with explicit time integration to solve the equations of solid dynamics for multimaterial media subjected to shocks and strong deformations, using material-specific EOS and constitutive models to close the system. ALEGRA also incorporates second-order-accurate interface tracking, remap algorithms that are third-order-accurate for pure material in one dimension, and stabilized "isentropic" multimaterial treatment [2]. ALEGRA and codes like it are often used to simulate systems where multiple materials interact in a environment of shock.

2.1. Lagrangian results

The problem is simulated first in the Lagrangian frame, using ALEGRA's standard contact algorithm [3] to control material interactions between the plates. The setup for the Lagrangian simulations is sketched in Figure 3. Each plate has thickness $T = 4$ cm and is resolved by N square elements in a one-element-thick 2D (quasi-1D) mesh. The problem is simulated on a series of seven meshes with increasing values of N, starting at $N = 20$ elements per plate, and doubling the mesh density up to to $N = 1280$.

Each plate is represented in the simulations with a unique material identifier, although the material properties are all identical. For the dissipationless case, the material response is simulated using a Mie-Grüneisen EOS model with a simple linear-elastic constitutive response. The Mie-Grüneisen parameters are given by $\rho_0 = 8930$ kg/m^3, $c_0 = 3940$ m/s, $C_V = 393.1$ J/kg/K,

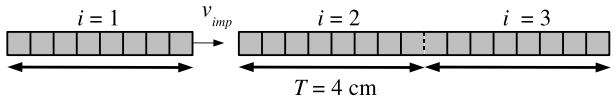

Figure 3: Setup for Lagrangian simulation of compound cohesionless impact problem with three plates of the same material.

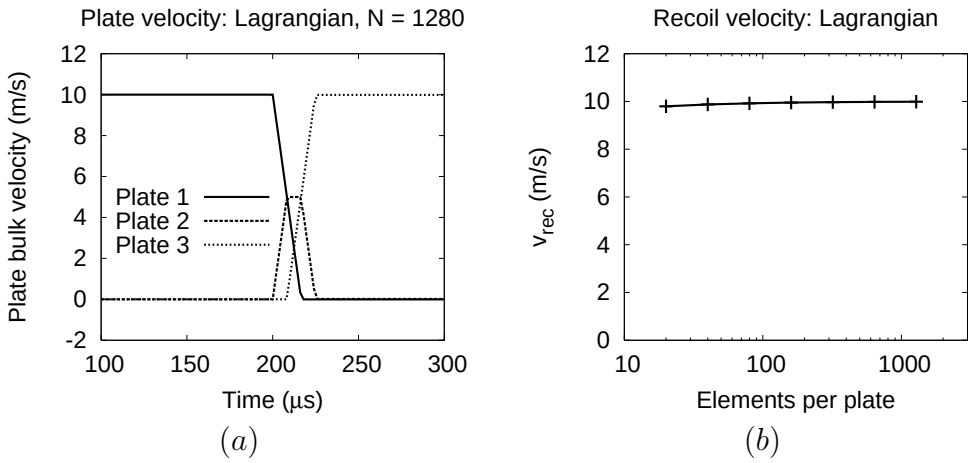

Figure 4: (a) Bulk plate velocities over time in Lagrangian simulation for the 10-m/s cohesionless impact problem in copper only, at $N = 1280$ elements per plate. (b) Recoil velocity for $20 \leq N \leq 1280$ Lagrangian simulations.

$s = 10^{-12}$, and $\Gamma_0 = 0$, where C_V is the specific heat capacity, The linear-elastic constitutive response is defined by Young's modulus $E = \rho_0 c_0^2 = 139$ GPa, and Poisson's ratio $\nu = 0.33$. To eliminate dissipative effects completely from this simple simulation, the artificial viscosity and hourglass control coefficients are also set to zero for the 10-m/s case.

Results for the bulk velocity of the three plates over time in the Lagrangian simulation at $N = 1280$ are shown in Figure 4(a). These velocities are measured as time-averages over the last 50 μs of the simulation. Here we see that, as expected, plates 1 and 2 come to rest after the impact event, and plate 3 recoils with a velocity nearly equal to v_{imp}. Further, the data in Figure 4(b) show that as the mesh is refined, the recoil velocity approaches the analytic value.

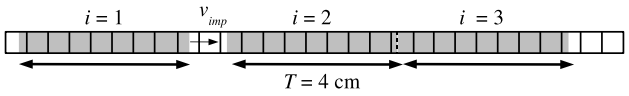

Figure 5: Setup for standard Eulerian simulation of compound cohesionless impact problem with three plates of the same material.

2.2. Eulerian results

The same set of simulations is repeated using the Eulerian frame in ALEGRA, which implies the use of the Lagrange-remap formulation, with interface tracking, multimaterial treatment in mixed elements, and third-order-accurate remap. In this case, the plates are overlaid on the Eulerian mesh at time zero, as shown schematically in Figure 5. The elements containing the material interfaces are therefore mixed elements. It is well known that the accuracy of standard Eulerian treatments is significantly compromised in situations where contact, slip, or gap opening/closure occurs within mixed elements [4]. Standard methods allow only a single stress and deformation within an element. Therefore, gap opening and relative motion between materials are inadmissible. Instead, erroneous material states can be introduced as the stress is changed in accordance with the motion. Ultimately, in the problem studied here, plates can neither fully join nor separate; plates 2 and 3 are effectively bonded.

This is demonstrated in the results for the Eulerian simulations at $v_{imp} = 10$ m/s, shown in Figure 6(a). Several errors are apparent. First, momentum transfer begins before the plate-1/plate-2 gap is closed, prior to $t = 200$ μs. Second, plates 1 and 2 both fail to come to rest. Finally, plate 3 never reaches the expected recoil velocity. Instead, plates 1, 2, and 3 remain effectively bonded after impact, and move forward with bulk velocities that oscillate in time as reverberating compression and release waves transfer momentum back and forth across the interfaces. Figure 6(b) demonstrates that this error does not diminish with mesh refinement.

3. Extended finite element method

In order to capture intra-element interface physics in the Eulerian frame with much greater fidelity, the extended finite element method (XFEM) has been implemented within ALEGRA as an alternative to the standard

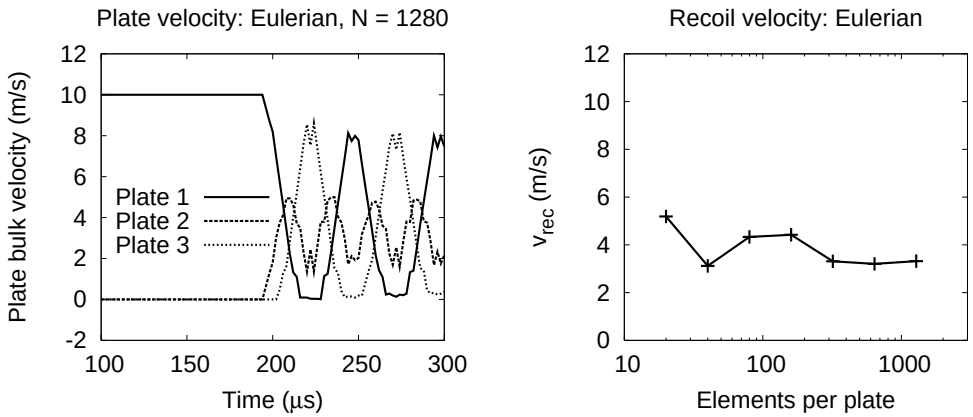

(a) (b)

Figure 6: (a) Bulk plate velocities over time in standard Eulerian simulation for the v_{imp} = 10-m/s cohesionless impact problem in copper only, at $N = 1280$ elements per plate. (b) Recoil velocity for $20 \leq N \leq 1280$ standard Eulerian simulations.

finite-element formulation and multimaterial treatment for Eulerian simulations. The central feature of the XFEM concept is "enrichment" of the finite-element approximation by incorporation of discontinuous fields into the basis functions and addition of degrees of freedom to make use of them [5]. XFEM has been implemented successfully in many other contexts for various applications [4, 6].

In ALEGRA's XFEM implementation, the finite-element basis functions in each multimaterial Eulerian element are enriched using Heaviside functions specific to each material. Additional degrees of freedom specific to each material are introduced at the nodes. [7, 8] Each material in an element then has an independent displacement field, so that contact, slip, and gap closure/opening can occur naturally in the Eulerian frame. A polygonal intersection remap algorithm is used with XFEM, including limiting for monotonicity preservation. First-order limiting only is employed in the present study, The Forward Incremement Lagrange Multiplier method of Carpenter *et al.* [9] is used to prevent interpenetration of materials. As described in Voth *et al.* [8], reconstructed interface segments and end-points act as faces and nodes, respectively. The constraint matrices are more complex than described in Reference [9], as they couple to all the nodes in the interface elements. An important implication of this algorithm is that the stable time

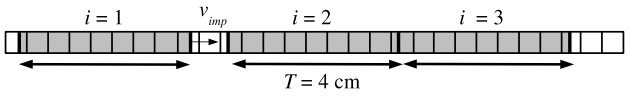

Figure 7: Setup for Eulerian XFEM simulation of compound cohesionless impact problem with three plates of the same material.

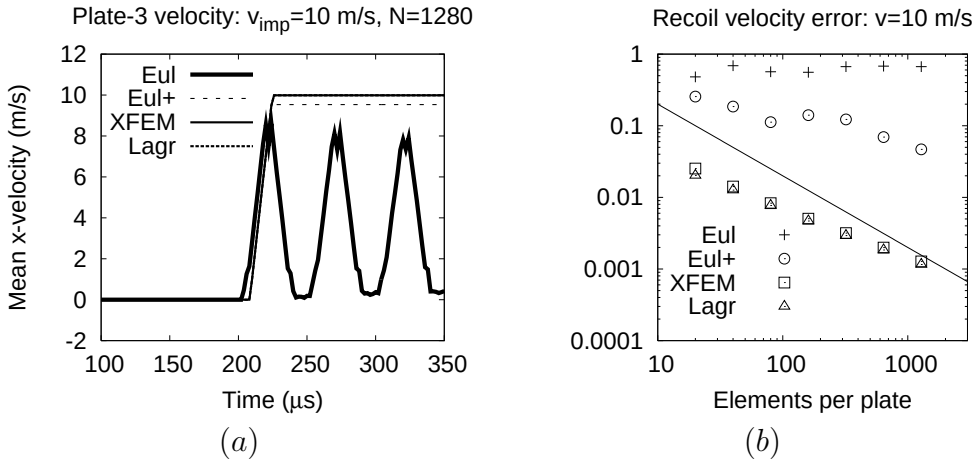

Figure 8: (a) Bulk plate-3 velocities over time for the 10-m/s cohesionless impact problem in copper only, at $N = 1280$ elements per plate. (b) Fractional error in recoil velocity with line indicating convergence at order 1.0.

step is unaffected by the size of the cut-element.

The 1D compound cohesionless impact problem is set up with XFEM in ALEGRA as shown in Figure 7. Material interface locations are encoded explicitly in the enriched basis functions, so that the domain has no mixed elements and the mesh, effectively, is locally body-fitted at interfaces.

The use of XFEM dramatically increases the accuracy of the results. Solutions for the 10-m/s case are shown in Figure 8. In the velocity histories for $N = 1280$, the XFEM and Lagrangian results nearly overlay each other. The standard Eulerian formulation, indicated by "Eul", fails to reach the full recoil velocity. In a second set of Eulerian simulations, methods are introduced to allow materials to separate by artificial insertion of void in interfacial elements under tension [2]. These methods are not a consistent algorithmic treatment of contact or gap closure/opening, and are often used

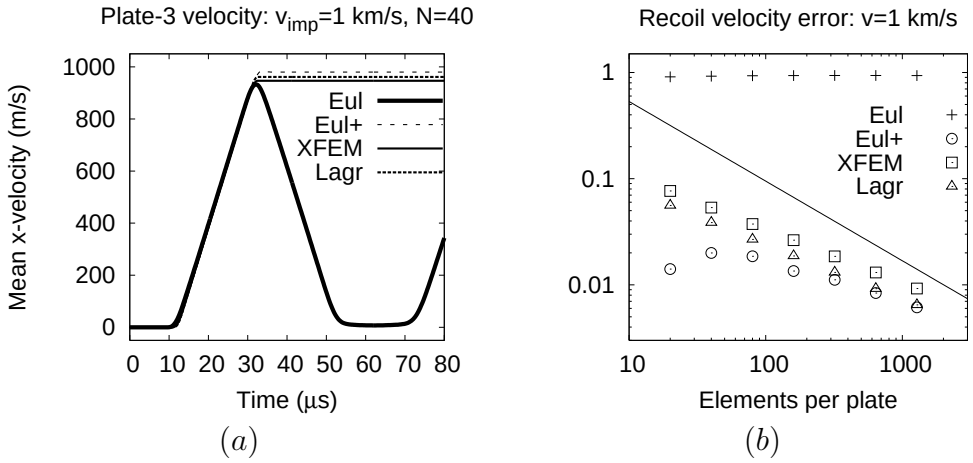

Figure 9: (a) Bulk plate-3 velocities over time for the 1000-m/s cohesionless impact problem in copper only, at $N = 40$ elements per plate. (b) Fractional error in recoil velocity with line indicating convergence at order 0.75.

in production calculations for pragmatic reasons. ALEGRA results computed in this way are indicated by "Eul+". The error with respect to the exact solution is computed as $\epsilon = (v_{imp} - v_{rec})/v_{imp}$ and plotted in Figure 8(b). These data show that monotonic convergence ($\epsilon \propto N^{-1}$) at a rate near unity with minimum error magnitude is only achieved by the XFEM and Lagrangian simulations.

A second version of the compound cohesionless impact problem is also simulated here, using $v_{imp} = 1000$ m/s, and the same material parameters for copper described above. The "dissipationless" setup is retained despite the higher velocity in this contrived problem, but the artificial viscosity coefficients are reset to their default values for this case. Results for the 1000-m/s case are shown in Figure 9. Velocity histories for $N = 40$ again show nearly overlying XFEM and Lagrangian results. Eulerian simulations again show non-separation of the target plates for the standard method, and in this case, the insertion of void in interfacial elements ("Eul+") yields *greater* recoil velocity than the Lagrangian method. Convergence data plotted in Figure 9(b) reveal that errors do not converge monotonically with artificial insertion of interfacial void, as seen in the 10-m/s case. This behavior is not acceptable from the perspective of verification. A line representing order-0.75 convergence is included for reference.

v_{imp}	Eul.	Eul.+	XFEM	Lagr.
10 m/s	-0.079	0.408	0.718	0.688
1000 m/s	-0.007	0.399	0.509	0.518

Table 1: Recoil-velocity error convergence rates: mean.

Mean convergence rates for both sets of simulations are shown in Table 1. For the "Eul+" cases where convergence is non-monotonic, rates are only computed in the smoothly converging region. The "Eul" and "Eul+" cases both fail to converge at the rate attained by the XFEM solutions. The XFEM and Lagrangian simulations converge at roughly order-0.7 at low impact velocity. Total momentum is conserved in all simulations here, but for high impact velocity, a rate of only about 0.5 is achieved. This is a consequence of the fact that at the higher impact velocity, the Mie-Grüneisen pressure-density response is no longer linear, even with the assumptions applied, so the "dissipationless" restriction is invalid.

4. Compound cohesionless impact problem: realistic

To eliminate the ambiguity in the foregoing analysis associated with the exclusion of dissipative effects, the problem described in Section 1 is extended to include the more realistic scenario where shock steepening ($s \neq 0$) and plasticity are active, and the dissipationless assumption can be abandoned. Further, it is extended to include impact between bodies of differing compositions. Here we consider the impact of a copper plate on a compound target consisting of a copper plate and an aluminum plate, joined as previously at a cohesionless interface. This is shown schematically in Figure 10.

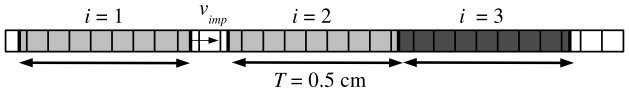

Figure 10: Setup for the two-material Eulerian XFEM simulation of compound cohesionless impact problem.

With these modifications, the graphical analysis used for the contrived dissipationless problem in Section 1 no longer applies. Instead, a method-of-characteristics-based technique can be used to track the transmission and

reflection of shock and release waves, and the motion of material interfaces and free surfaces. A method of this type has been implemented in SWAP-9 [10], which uses a formulation that is second-order-accurate in the strain increment. SWAP-9 can be used for arbitrary EOS and constitutive models.

For this more realistic two-material impact problem, standard Mie-Grüneisen parameters are used for copper and aluminum, along with an elastic-perfectly-plastic constitutive model using standard parameters. These parameters, including the yield stress Y, are listed in Table 2. As previously, in the elastic regime, a Young's modulus $E = \rho_0 c_0^2$ is used.

	Cu	Al
ρ_0 (kg/m^3)	8930	2707
c_0 (m/s)	3940	5250
Γ_0	1.99	1.97
s	1.489	1.370
ν	0.355	0.334
Y (MPa)	89.7	265.0

Table 2: Material parameters used in realistic two-material cohesionless impact problem.

The two-material cohesionless impact problem is solved for a plate thickness $T = 0.5$ cm and an impact velocity $v_{imp} = 100$ m/s. The resulting wave diagram computed by SWAP-9 is shown in Figure 11. The outcome is a bulk plate-3 recoil velocity of 127.22 m/s, which exceeds the impact velocity because of the lower shock impedance of aluminum relative to copper.

ALEGRA simulations are configured using the same material parameters, on the same sets of meshes described in Sections 2 and 3. Simulation results for the standard Eulerian and XFEM cases are shown in Figure 12. Similarly to the dissipationless case, separation does not occur in the Eulerian simulations without the use of artificial interfacial void. Convergence trends for spatial refinement are shown in Figure 13. Errors are computed with respect to the SWAP-9 reference solution. Here we observe that even with real material parameters including plasticity and a full Mie-Grüneisen EOS representation, the XFEM implementation in ALEGRA still converges toward the reference solution at nearly the same rate, and with nearly the same error magnitudes, as the Lagrangian case. The standard Eulerian solution, as expected, fails to converge. With artificial interfacial void ("Eul+"), the recoil velocity overshoots the reference solution and dramatic oscillations are seen

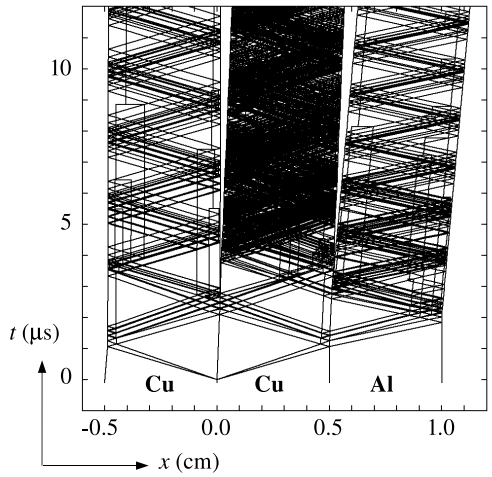

Figure 11: Wave diagram for 100-m/s impact of copper plate on compound cohesionless copper-aluminum target, computed using SWAP-9.

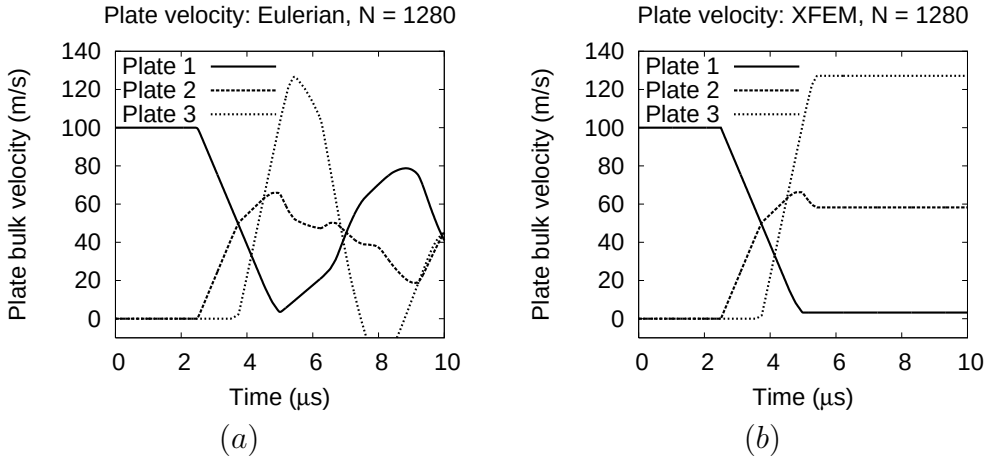

Figure 12: Bulk plate velocities over time in (a) standard Eulerian simulation and (b) XFEM simulation for the 100-m/s cohesionless impact problem with real material properties and a copper/aluminum target.

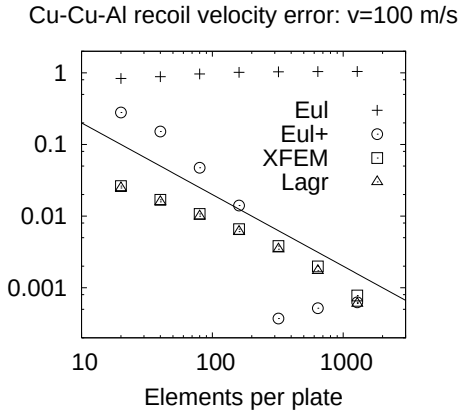

Figure 13: Fractional error in recoil velocity for the v_{imp} = 100-m/s impact on a copper/aluminum target. Line indicates first-order convergence with respect to reference solution from SWAP-9.

in the error trend. Only with XFEM is Lagrangian quality retained, with monotonically diminishing error, maximum convergence rate, and minimum error magnitude. The mean convergence rates are the following: Eulerian, -0.054; XFEM, 0.845; and Lagrangian, 0.893.

5. Conclusions

The verification study carried out here indicates that the XFEM implementation in ALEGRA faithfully captures features of impact-induced material separation in the Eulerian frame with accuracy very near near to that of the pure Lagrangian formulation. Rigorous verification bears out this observation, showing that XFEM is the only Eulerian treatment providing acceptable convergence behavior. We conclude that XFEM shows tremendous promise for use in multimaterial shock-hydrodynamics modeling.

Acknowledgments: the authors wish to thank the U. S. Army Research Laboratory and Dr. Tracy Vogler (Sandia National Laboratories).

References

[1] Robinson AC, Rider WJ, et al. ALEGRA: An arbitrary Lagrangian-Eulerian multimaterial, multiphysics code. In: Proceedings of the 46th AIAA Aerospace Sciences Meeting, Reno, NV. 2008,AIAA-2008-1235.

[2] Robinson AC, et al. ALEGRA user manual: version 5.0. Tech. Rep.; Sandia National Laboratories; Albuquerque, NM; 2010. SAND2010-4796.

[3] Taylor LM, Flanagan DP. PRONTO 3D: A three-dimensional transient solid dynamics program. Tech. Rep.; Sandia National Laboratories; Albuquerque, NM; 1987. SAND87-1912.

[4] Vitali E, Benson DJ. An extended finite element formulation for contact in multi-material arbitrary Lagrangian-Eulerian calculations. Int J Numer Meth Engng 2006;67:1420–44.

[5] Dolbow J, Moës N, Belytschko T. Discontinuous enrichment in finite elements with a partition of unity method. Finite Elem Anal Des 2000;36:253–60.

[6] Yazid A, Abdelkader N, Abdelmadjid H. A state-of-the-art review of the X-FEM for computational fracture mechanics. Appl Math Model 2009;33:4269–82.

[7] Dolbow J, Mosso SJ, Robbins J, Voth TE. Coupling volume-of-fluid based interface reconstructions with the extended finite element method. Comput Methods Appl Mech Engrg 2008;197:439–47.

[8] Voth TE, Robbins J, Mosso SJ. An implementation of the X-FEM for arbitrary Lagrangian Eulerian (ALE) mechanics; 2009. 10th U. S. National Congress on Computational Mechanics, Columbus, OH.

[9] Carpenter NJ, Taylor RL, Katona MG. Lagrange constraints for transient finite element surface contact. Int J Numer Meth Engng 1991;32:103–28.

[10] Barker LM, Young EG. SWAP-9: An improved stress wave analyzing program. Tech. Rep.; Sandia National Laboratories; Albuquerque, NM; 1974. SLA-74-0009.